ADVANCED ENGINEERING MATERIALS
www.aem-journal.com

Effect of Relatively Low Levels of Porosity on the Plasticity of Metals and Implications for Profilometry-Based Indentation Plastometry

*Rebecca Reiff-Musgrove, Wenchen Gu, Jimmy E. Campbell, John Reidy, Animesh Bose, Aadithya Chitrapur, Yuanbo Tang, Max Burley, and Trevor William Clyne**

Herein, the effect of dispersed (relatively low levels of) porosity within a metal on its plastic deformation is examined. Stainless steel samples, made via additive manufacturing, are used in the work. It's found that porosity reduces stress levels during yielding and work hardening, approximately in proportion to the pore content. There is no significant difference between the strength of the effect during tension and compression, although porosity does reduce the tensile ductility. Finally, the profilometry-based indentation plastometry (PIP) methodology (for obtaining stress–strain curves from indentation testing) are used. Porosity tends to bring the inferred yield stress down more strongly than during tensile testing and give higher initial rates of work hardening. This is associated with high local strains near the indenter causing closure of pores, so that volume is not conserved during the test. The resultant reduction in the pile-up around the indent creates errors in the inferred stress–strain curve.

1. Introduction

Porosity is not uncommon in certain types of metallic components, particularly castings. Furthermore, while most rolled, extruded, and forged products can usually be taken to be pore free, many powder-route components, including some produced via additive manufacturing (AM), do contain at least some porosity. Moreover, while porosity in castings can be coarse and inhomogeneously distributed, that in powder route products is often relatively fine and well dispersed. In fact, for certain types of product, particularly in bearing applications, this is deliberate as it can assist in retention of lubricants.

High porosity levels, and coarse pores, sometimes concentrated into certain regions, are likely to impair mechanical properties, particularly fracture characteristics. However, there is interest in the effect on mechanical properties of the presence of (uniformly-distributed) pores, at relatively low levels, of the order of a few %. Previous study of this has been somewhat limited. Several workers have compared stress–strain curves before and after the application of a hot isostatic pressing (HIP) treatment (designed to remove the porosity). Unfortunately, in most such studies, the heat treatment associated with the HIP operation also induced other microstructural changes—often having stronger effects on the mechanical response than those due to removal of the pores. For example, Hirata et al.[1] tested Al-based AM samples produced under different conditions—such that the porosity level ranged up to about 3–4%. They found that the yield stress was similar for them all, at about 250 MPa, but that higher porosity levels gave lower ductility and reduced ultimate tensile strength (UTS) levels (ranging from 300 to 500 MPa), that is, they became more brittle as the porosity level was raised. HIPing of these materials brought the YS down to 100 MPa, and the UTS to 150 MPa, but with much higher ductility values. The HIP operation evidently changed the microstructure—probably causing overaging—as well as eliminating the pores. Broadly similar outcomes have also been reported by several other groups.[2–5]

Among the specific issues of interest are the possibility of tensile compressive asymmetry (TCA), that is, a stress–strain curve that is different when a sample is tested (in a particular direction) in uniaxial tension and uniaxial compression. While genuine TCA is relatively rare, it does occur in certain cases, notably in highly textured hexagonal metals that exhibit extensive deformation twinning.[6] It effectively reflects a dependence of the

R. Reiff-Musgrove, W. Gu, J. E. Campbell, M. Burley, T. W. Clyne
Plastometrex Ltd.
204 Science Park, Milton Road, Cambridge CB4 0GZ, UK
E-mail: b.clyne@plastometrex.com

J. Reidy, A. Bose, A. Chitrapur
Desktop Metals
63 3rd Avenue, Burlington, MASS 01803, USA

Y. Tang
Department of Materials
University of Oxford
Parks Road, Oxford OX1 3PH, UK

T. W. Clyne
Department of Materials Science
University of Cambridge
27 Charles Babbage Road, Cambridge CB3 0FS, UK

The ORCID identification number(s) for the author(s) of this article can be found under https://doi.org/10.1002/adem.202200642.

DOI: 10.1002/adem.202200642

stress–strain curve on the hydrostatic component of the applied stress, rather than just the von Mises stress, which is the basis for almost all plasticity modeling. Plastic deformation of metals usually occurs at constant volume, so that the hydrostatic stress is not normally expected to have any effect. However, if the plasticity has an associated volume change, then this may not be the case. For example, TCA has been reported[7–10] in metastable austenitic stainless steels, in which plasticity commonly involves the formation of martensite, that is, a phase change (with an associated volume change) takes place. The presence of porosity, which might be expected to be raised during plastic deformation by a tensile hydrostatic stress and decreased by a compressive one, could therefore lead to a TCA effect.

Despite this being a fairly well-defined expectation, there has been little systematic study of it. However, Deng et al.[11] did claim to detect TCA in sintered steel samples containing up to 10% porosity. They reported lower yield stress values in tension than in compression, falling from about 195–180 MPa with 3.5% porosity and 185–165 MPa with 4.7% porosity. For 10% porosity, the fall was from about 180 MPa (compression) to 130 MPa (tension). However, this work was cent red on cyclic loading, with a (total) strain range of only ±1%. The strain was measured remote from the sample and the onset of yielding was quite gradual, so the yield stress values obtained may be subject to significant error. No measurements were made on corresponding pore-free material. The authors rationalized the observed behavior largely in terms of crack growth. This will certainly be relevant to failure, but it might have been expected that yielding would not involve cracking, at least for relatively low porosity levels. Nevertheless, this work does report a systematic trend for yielding to occur at lower stresses in tension than in compression for porous materials and for the difference to be greater with higher porosity levels. In fact, similar results, based on similar experiments, were reported[12] two years earlier, although the difference between tensile and compressive yield stresses was lower and the porosity level was not measured.

There has been interest in modeling of the effect of porosity on plastic deformation. The main efforts in this direction have been based on the work of Gurson.[13] His paper, which was oriented toward void nucleation and growth (leading to ductile rupture), provided an expression for the yield stress, as a function of porosity level. (A second planned paper, concerning work hardening, apparently never materialized.) It takes no account of any possible TCA, and indeed it is apparently aimed solely at tensile loading (and hence a tensile hydrostatic stress). The material is thus treated as a "porous von Mises" one. Several (more recent) studies[14–18] have picked up on the Gurson model and attempted to develop it in various ways, although much of this work has still been oriented toward void growth and its relevance to failure rather than being focused specifically on the effect of porosity on plasticity. Nevertheless, some of these models have been incorporated into certain commercial finite-element method (FEM) packages. The mechanistic basis for these formulations is rather unclear, and in general they are not directly applicable to compressive loading.

Among other relevant modeling activities are some aimed at FEM simulation of the effect of dispersed pores on local stress and strain fields and on overall average stress–strain relationships. For example, Shen and Brinson[19] did work of this type on porous titanium, generating random spatial distributions of spherical pores with given size distributions and a porosity level of 15%: this was described as "low" (for a metallic foam), although, for a porous metallic component, it would be considered high. They carried out both 2D (plane strain) and 3D modeling, with their main conclusion being that the former is likely to be unreliable. They explored only low overall strain levels (1%), but, with this high porosity level and a random spatial distribution, even this level can lead to high local strains (>10%). In practice, such regions would tend to rupture, but this was not considered. There was also no study of possible TCA effects. In general, theoretical studies of this type have limited relevance to the higher strain/lower porosity regimes of interest here.

The current work involves study of the effect of porosity level on the mechanical response of stainless steel samples, made using a 3D printing process, with and without a subsequent HIP operation to remove the porosity. While some AM processes may lead to pores with a variety of shapes and spatial distributions, this technique tends to produce isolated, spherical pores that are randomly distributed. The work also involves profilometry-based indentation plastometry (PIP), which is now starting to enter the mainstream of mechanical testing procedures. It is based on iterative FEM simulation of the indentation process, with the plasticity parameters (in a constitutive law) being repeatedly changed until optimal agreement is reached between measured and predicted residual indent profiles. Integrated facilities are now commercially available, allowing stress–strain curves to be obtained from a single indentation experiment within a few minutes. A recent review[20] covers various aspects of the procedure and its implementation. It has been applied[21] to AM material (exhibiting anisotropy, but no porosity). There is therefore interest in exploring and understanding how the presence of (relatively low levels of) porosity is likely to affect outcomes for this type of test and in checking on how these relate to results obtained via conventional uniaxial testing.

2. Microstructure

SEM images of the typical polished surfaces of HT-2 and HIP/HT-1 samples are shown in **Figure 1**. Only the former (Figure 1a) shows any obvious pores. These are apparently isolated, reasonably well dispersed, and approximately spherical (with diameters of around 5–10 μm). While measuring porosity contents via image analysis of polished sections is notoriously inaccurate, this micrograph is consistent with the level being of the order 1–2%. These microstructures are largely martensitic. The slightly darker regions are thought to be ferrite, although distinguishing the ferritic and martensitic phases is a little difficult, as they have very similar composition and crystallography. The small, bright constituents are carbides.

The EBSD images shown in **Figure 2** indicate that the martensite laths are relatively coarse and also confirm the broad similarity of the microstructures produced with and without the HIPing operation. Also, there is no obvious texture in either case.

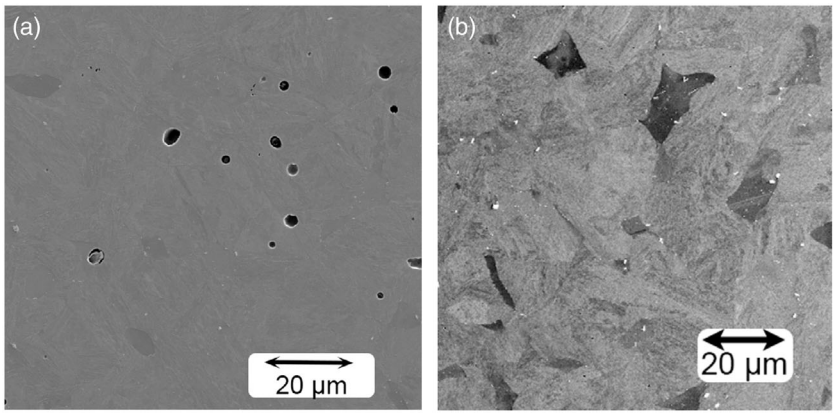

Figure 1. SEM images of a) an HT-2 sample and b) an HIP/HT-1 sample.

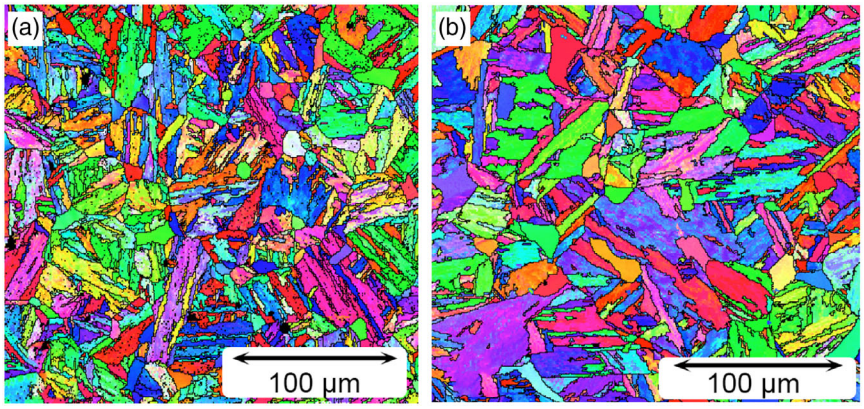

Figure 2. EBSD images of a) an HT-2 sample and b) an HIP/HT-1 sample.

3. Mechanical Characteristics

3.1. Tensile Testing

Tensile (nominal) stress–strain curves, for the three types of sample, are shown in **Figure 3**. (Representative single curves are shown in each case: in general, repeats tend to fall within bands of about ±1%. At least for yield stress and UTS, there tends to be slightly more variation in ductility values.) A trend is apparent, in the form of slightly increasing YS and UTS as the porosity level is reduced. A similar trend is observed for ductility but with the dependence being considerably stronger. Such a dependence of the final rupture event on the prior presence of pores is certainly not unexpected.

It is noticeable, however, that the effect on yield stress and UTS is small. As a very crude approximation, these are raised by about 1% (≈15 MPa) for each percent reduction in porosity level, at least over this narrow range. The change is thus close to just being in proportion to the average change in sectional area, although it should be emphasized that the experimental scatter is similar in magnitude to this, so the main point to note is simply that these levels of porosity have only a very limited effect on the plastic deformation characteristics. However, that is not the case for ductility, which is more sensitive to the porosity level.

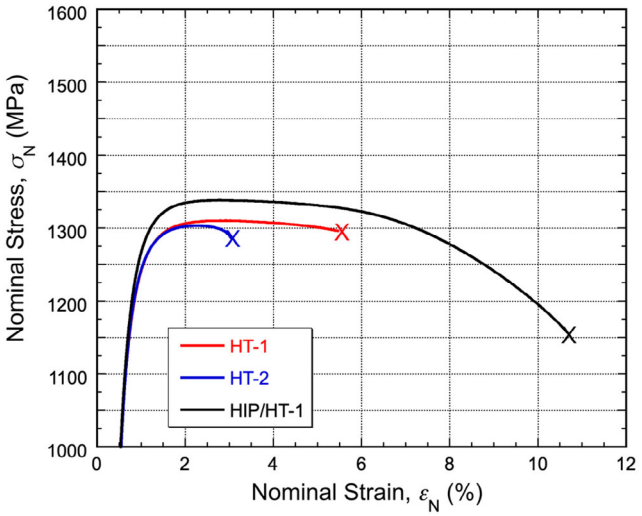

Figure 3. Tensile (nominal) stress–strain curves for the three types of sample tested. (In this and following plots, the origin has been displaced to a stress level of 1000 MPa.).

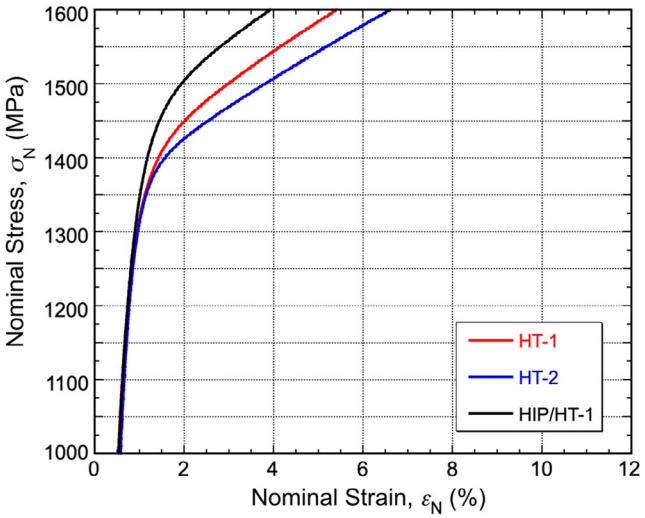

Figure 4. Compressive (nominal) stress–strain curves for the three types of sample tested.

3.2. Compressive Testing

Corresponding compressive stress–strain curves are shown in **Figure 4**. These show similar trends to those of the tensile curves. There is again a small, but progressive, increase in yield stress with decreasing porosity level. Something like 1% change for each percent of porosity is again approximately observed, although there is always an issue concerning exactly how a yield stress is defined. Of course, there are no UTS or ductility values, but the work hardening characteristics are again similar.

While the observed trends are thus consistent between compressive and tensile tests, and the yield stress values appear to be in the same broad range, accurate assessment of whether there is any TCA requires both sets of plots to be converted to true stress–true strain curves: if there is no TCA, then the two curves should coincide. This conversion is readily done for tension (up to the onset of necking), using the standard analytical equations. However, under compression these relationships do not accurately hold since friction affects the measured (nominal) stress–strain relationship. Converted plots for compression have been obtained both by using the equations and via an inverse FEM method, changing the plasticity parameters in the Voce law until optimum agreement is reached between the measured nominal curve and the outcome of the FEM simulation of the test. This was done using a friction coefficient value of 0.15, which is broadly in line with the outcome of previous work[24] for these conditions (with no lubrication).

The sets of true stress–strain curves obtained in this way, that is, via the analytical equations for the tensile data and via both methods for the compression curves, are shown in **Figure 5**. The FEM simulations (using Voce parameter sets) always involve a discrete yield point, so the gradual transition regime that is sometimes observed in practice cannot be captured. This is apparent in the FEM-obtained compression curves in Figure 5. It can be seen in Figure 5a that taking account of the effect of friction during compression testing in this way brings the curves down by an increment of ≈50 MPa. They nevertheless still lie slightly above the corresponding tensile curves. However, this is the case for the pore-free material, as well as for the porous samples—in fact, if anything, the discrepancy is greater for the pore-free material. It's therefore clear that there is no TCA arising from the presence of porosity, at least for these relatively low levels. In other words, while the porosity makes the material a little softer, there is no significant difference between the extent of this during tensile and compressive loading.

It could be concluded from Figure 5 that there is a (very small) TCA effect for all these materials, although this can probably be regarded as within general experimental error. (The discrepancy

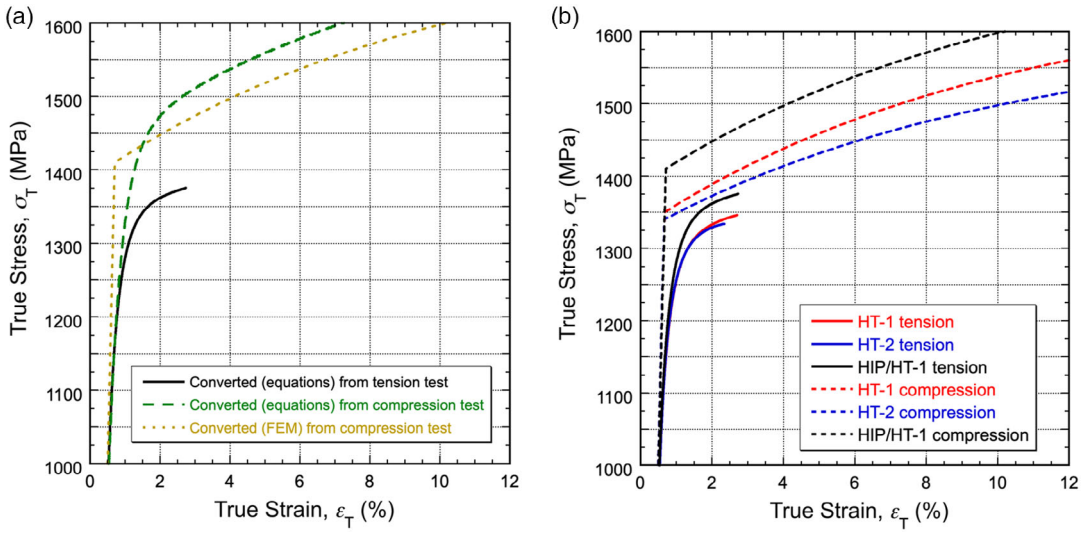

Figure 5. True stress–strain curves for uniaxial tension and compression, showing a) the effect of the type of conversion for HIP/HT-1 samples and b) comparisons for all three materials, showing the analytical equation conversions for tensile and the inverse FEM conversions for compression.

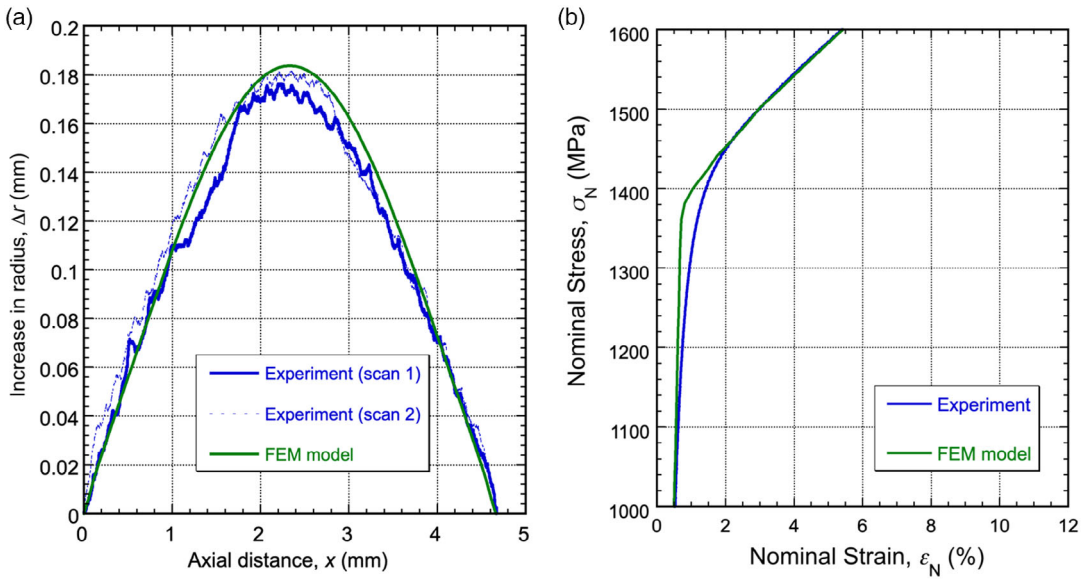

Figure 6. Comparisons between experiment and FEM model (with $\mu = 0.15$) for compression testing of sample HT-1, showing a) barreling profiles (scans on both sides of the sample) and b) nominal stress–strain curves.

is only of the order of 5%, which is typically regarded as being within a normal error band for repeating of a mechanical test.) It's certainly not easy to correct accurately for the effect of friction during compressive loading. For example, in practice the friction coefficient, μ, may vary during the test. A useful way of cross-checking is to compare measured and modeled barreling profiles and such a comparison is shown in **Figure 6**a for the HT-1 sample (using $\mu = 0.15$). The agreement, both for this and for the nominal stress–strain curve (Figure 6b) is quite good, so this value can at least be regarded as appropriate as an average.

3.3. PIP Testing

A measured set of indent profiles, for the three cases, is shown in **Figure 7**. These indents are all radially symmetric, indicating isotropy (in the plane concerned). In fact, much the same profiles were obtained in other planes, so that these materials can be treated as completely isotropic. This is consistent with the non-directional nature of the manufacturing process. It may be noted that the penetration is deeper for porous materials. Furthermore, the pile-up heights are lower. Both effects will be reflected in the inferred stress–strain curves.

The corresponding set of (true) stress–strain curves is shown in **Figure 8**a. On comparing these with the plots in Figure 5b, it's clear that the broad trends are being captured correctly, for example, the yield stress is being progressively reduced as the porosity level is raised. Also, for the fully dense material, the yield stress and work hardening characteristics are well captured. However, in quantitative terms, there is a discrepancy for the porous materials. This can be seen in Figure 8b, which compares the nominal tensile stress–strain plots from direct tensile testing with those obtained from PIP. The PIP-inferred yield stresses for the porous materials are below those observed in uniaxial testing. For example, the presence of about 2% of porosity has brought it down

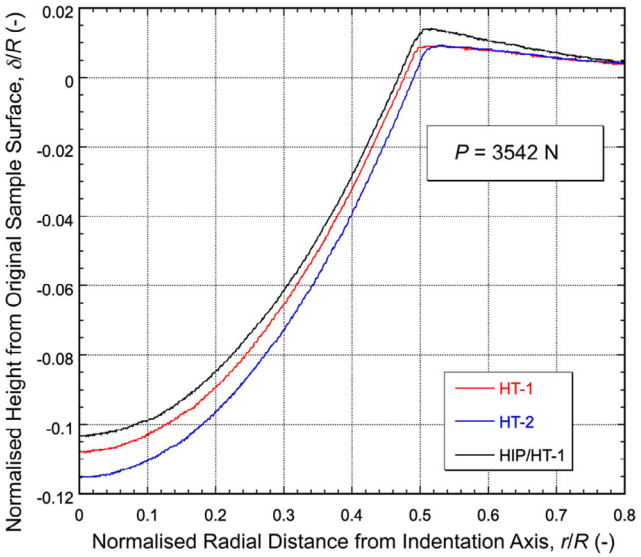

Figure 7. Typical measured residual indent profiles for the three types of sample.

from about 1350 MPa to around 1100 MPa, whereas the uniaxial data indicate a drop of no more than 50 MPa. Also, the PIP-inferred work hardening rates (WHRs) for the porous samples are too high. Leaving aside the short initial transients, these materials do not in fact work harden very much. This is captured correctly for the pore-free material, but not for the porous ones.

In fact, this outcome is not unexpected. The indentation test stimulates relatively high plastic strains, particularly in regions close to the indenter. During these uniaxial tests, on the other hand, the strains have remained relatively low, particularly for the tensile tests (prior to the onset of necking). Since the

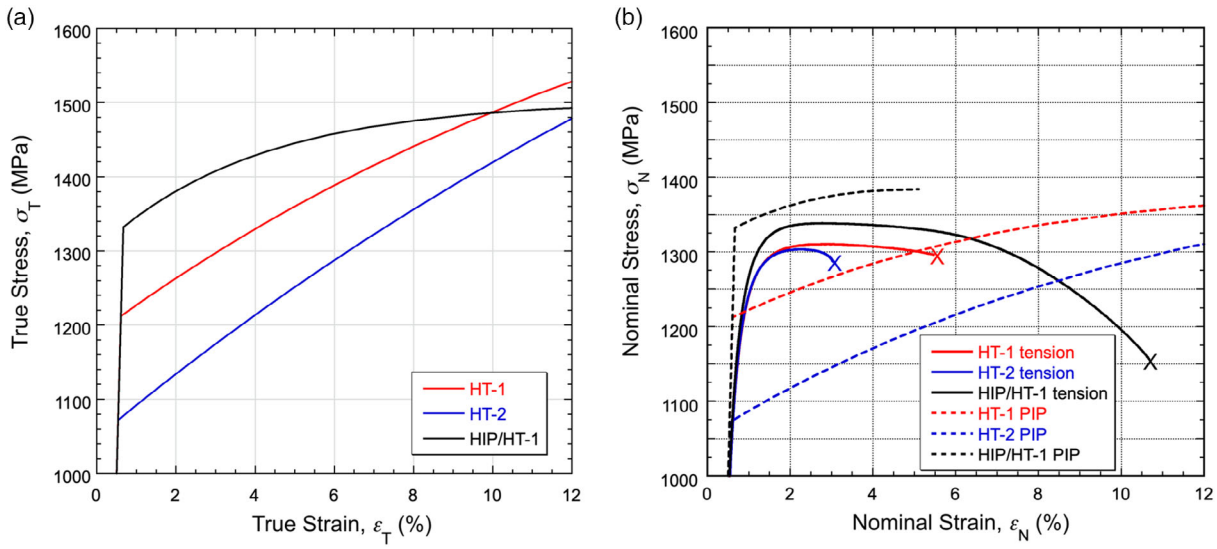

Figure 8. Stress–strain curves for all three materials, showing a) PIP-derived true stress–true strain relationships (Voce plots for best fit sets of parameter values) and b) a comparison, for tensile loading, between directly measured and PIP-derived nominal stress–nominal strain curves. (The PIP-derived curves are shown only up to the predicted onset of necking.).

hydrostatic stress is predominantly compressive during indentation, pores (near the indenter) are likely to become closed during PIP testing. This will tend to make the material appear softer, that is, to have a lower inferred yield stress than during uniaxial testing. Furthermore, as volume is not now being conserved, the pile-up will tend to be lower, leading to the inference of an erroneously high work hardening rate. As it happens, the PIP-inferred UTS values agree quite well with the tensile ones for the porous materials, but the necking strains are being overestimated and in general the early parts of the curves are not well captured or at least they are not up to the accuracy generally expected of PIP testing.

4. Conclusion

The following conclusions can be drawn from this work, which has involved experimental study of the stress–strain relationships exhibited by three materials that differ only in the level of (relatively fine, well dispersed) porosity within them (in the range 0–2%). 1) The presence of porosity results in slight softening (reduction in yield stress and subsequent flow stress), although this is only in approximate proportion to the porosity level, that is, 1% of porosity leads to reduction in yield stress of around 1%. 2) The ductility is more strongly affected by the presence of porosity, presumably because it accelerates the process of void nucleation and growth that precedes fracture (in relatively ductile materials). The nominal strain at fracture during tensile testing (for the sample geometry concerned) is reduced from around 10% to about 3% by the presence of porosity at a level of 2%. The strength of the effect could be greater for coarser pores (which have not been covered in this work). 3) The effect of these levels of porosity on the plasticity response is much the same for tensile and compressive loading, that is, no tensile-compressive asymmetry (TCA) has been detected. 4) Application of the PIP procedure to materials with these levels of porosity tends to give rise to error, in the form of the inferred yield stress values being lower than those obtained by conventional uniaxial testing and the initial work hardening rate being somewhat higher. This probably arises from closure of pores in the high-strain regions close to the indenter, which allows increased penetration and also reduces the degree of pile-up (as volume is no longer being conserved). It may therefore be concluded that, while PIP can be applied to porous materials, the results may be subject to significant error. At present, there is no well-defined way of compensating for this, apart from noting the general nature of the expected effects.

5. Experimental Section

Production of Material: Samples were produced by Desktop Metal, using an SPJ Binder Jet Printer. The base material was 17-4 PH stainless steel powder produced by nitrogen gas atomization, with a D90 of 25 μm. Binder jet 3D printing of metals involves: 1) printing the geometry (using a metal powder and a binder), 2) curing to improve the "green" strength, 3) depowdering, 4) binder removal, and finally 5) consolidation via a high-temperature sintering process.[22,23] The first step spread a thin layer (typically 30–150 μm) of metal powder, either by a "bed-to-bed" process or by a powder metering and compaction scheme. A printhead then traversed the bed, applying binder in regions defined by the part geometry. The build bed was then lowered by the layer height and this powder spread and binder jetting was repeated to build up the desired geometry. Desktop Metal utilized a variation of binder jetting called single-pass jetting (SPJ).[23] In this process, each step of printing was conducted in a single pass, enabling layer times of <3 s and hence very high build rates. Once the printing step was complete, the build bed was subjected to a thermal step to drive off residual solvent from the binder and improve the green strength. After curing, the green parts were excavated from the bed and excess unbound powder was removed in a depowdering process. The green parts typically contained 1–2 wt% polymer, which needed to be removed prior to the sintering step.

Debinding is typically performed by heating to the thermal decomposition temperature of the polymer. Once the polymer has been removed, the parts may be sintered by heating to a high temperature (below the solidus of the metal) in controlled atmosphere (inert, reducing, or vacuum, depending on the alloy). After sintering, the parts often contain a small level of fine, well-dispersed porosity. Green parts were printed using a layer thickness of 65 μm and subsequently cured in inert atmosphere at 200 °C. The green parts were debound and sintered using a multistep heating profile in a metal hot-zone furnace. The standard procedure creates samples with a typical porosity level of around 1%—in the form of relatively small, isolated, uniformly distributed pores. Samples were also produced using a modified procedure, involving a sintering temperature that was reduced by 40 °C. These had a similar pore architecture, but with a slightly higher porosity level, typically around 2%. These two types of material were thus given designations that terminated with "−1" or "−2".

Heat Treatment and Hot Isostatic Pressing: A key objective of the work was to study the effect of (relatively low levels of) porosity, isolating it from the influence of other microstructural features. The obvious way to remove porosity was by HIPing, but there was a likelihood that the associated heat treatment would affect the microstructure in other ways. The approach adopted was therefore to first apply the HIPing heat treatment (without pressure) to the (porous) samples that were not HIPed. This was followed by an age-hardening heat treatment. This same age-hardening treatment was also applied to the HIPed samples. The samples were therefore designated HT-1, HT-2, and HIP/HT-1, with, as outlined earlier, the number indicating the nominal porosity level (in %) of the samples (before any HIPing).

The aging sequence involved solution treatment at 900 °C, followed by holding for 4 h at an aging temperature of 480 °C. The HIPing operation, done by Bodycote HIP Ltd (Chesterfield), was carried out at 1120 °C, with an applied pressure of 103 MPa, for 240 min. There was no encapsulation, so any surface-connected porosity would not have been removed by HIPing. Although it's not expected that much of the porosity in these samples would have been surface connected, a grinding operation was carried out to remove near-surface regions before any characterization or mechanical testing was carried out.

Measurement of Porosity Levels: Porosity levels were measured by hydrostatic weighing, with the immersion liquid being Flutec PP9 (density, $\rho_L = 1.972\ \mathrm{g\ mL^{-1}}$). The density of the sample is given by

$$\rho_s = \rho_L \frac{w_1}{w_2} \tag{1}$$

where ρ_L is the density of the liquid, w_1 is the weight of the sample, and w_2 is the weight of the displaced liquid. (This the difference between the weight of the beaker + liquid, with and without the sample suspended in it—supported via a fine thread.) The porosity values were obtained by taking the average density for the HIPed samples ($7.7713\ \mathrm{g\ mL^{-1}}$) to be the correct full density for this alloy. The average porosity values for HIP/HT-1, HT-1, and HT-2 were therefore 0 (by definition), $0.3\% \pm 0.2\%$, and $1.7\% \pm 0.2\%$. The latter two values were slightly below the nominal values of 1% and 2%, and there was quite a lot of scatter. This was probably in part due to measurement error and in part due to sample-to-sample variation. In any event, it should be recognized that, while the objective of having a set of pore-free samples, plus other samples with porosity levels of around 1–2%, was met, these levels were not very well defined. This should be borne in mind when interpreting other results.

Microstructural Examination: Microstructure was characterized using a Zeiss Merlin field-emission gun–scanning electron microscope (FEG-SEM) equipped with a Bruker electron backscattered diffraction (EBSD) detector. The steel samples were prepared using standard metallurgical procedures involving grinding and polishing down to 1 μm diamond suspension. The finishing step was carried out with colloidal silica for 5 min. The specimens were examined by SEM with an acceleration voltage at 15 kV using a secondary electron detector to reveal pores. The EBSD patterns were acquired at a step size of 0.7 μm and stored in a resolution of 160×120 pixels. ESPRIT 2.1 software was used for postprocessing the Kikuchi patterns collected. Various phases were made available for indexing, including bcc α (ferrite), fcc γ (austenite), and bcc δ. Only the bcc α (ferrite) phase was successfully indexed in all samples.

Uniaxial Testing: Uniaxial testing was carried out using an Instron 3369, with 50 kN capacity. Tensile samples had a reduced section length of 30, 5 mm square, with a clip gauge of length 25 mm. Compression samples were in the form of cylinders (5 mm diameter and 5.5 mm long). No lubricant was used. Displacement was measured using a linear variable displacement transducer (LVDT) attached to the upper platen and actuated against the lower one. In addition, strain gauges were attached to both sides of the sample. Outputs from these were used to correct for compliance in the LVDT measurements by matching the strains in the elastic portion of the test.

Indentation Plastometry: Three steps are involved in obtaining a true stress–true strain curve from a PIP test. These are 1) pushing a hard spherical indenter into the sample with a known force, 2) measuring the (radially symmetric) profile of the indent, and 3) iterative FEM simulation of the test until the best fit set of (Voce) plasticity parameter values is obtained. This (true) stress–strain relationship can be used to obtain outcomes from other types of loading configurations, including uniaxial testing. For tensile testing, the nominal stress–strain relationship, up to the onset of necking, can be obtained using the well-known analytical relationships. Beyond that point, FEM simulation of the test would be needed. For compression testing, such simulation (with a known coefficient of friction) is needed from the start, although the effect of friction is often relatively small and its general effect, that is, to raise the stress needed to produce a given strain, is always the same.

Acknowledgements

Relevant support for TWC was received from EPSRC (grant EP/I038691/1) and from the Leverhulme Trust, in the form of an international network grant (IN-2016-004) and an Emeritus fellowship (EM/2019-038/4).

Conflict of Interest

The authors declare no conflict of interest.

Data Availability Statement

The data that support the findings of this study are available from the corresponding author upon reasonable request.

Keywords

Gurson model, indentation plastometry, inverse finite-element method, porosity

Received: May 2, 2022
Revised: June 16, 2022
Published online:

[1] T. Hirata, T. Kimura, T. Nakamoto, *Mater. Sci. Eng. A* **2020**, *772*, 138713.
[2] E. Hernandez-Nava, C. J. Smith, F. Derguti, S. Tammas-Williams, F. Leonard, P. J. Withers, I. Todd, R. Goodall, *Acta Mater.* **2015**, *85*, 387.
[3] C. B. Finfrock, A. Exil, J. D. Carroll, L. Deibler, *Metall. Microstruct. Analysis* **2018**, *7*, 443.
[4] T. Cegan, M. Pagac, J. Jurica, K. Skotnicova, J. Hajnys, L. Horsak, K. Soucek, P. Krpec, *Materials* **2020**, *13*, 4377.
[5] R. M. Kumar, B. R. Golla, *Trans. Indian Inst. Metals* **2021**, *74*, 2379.
[6] Y. T. Tang, R. Reiff-Musgrove, W. Gu, J. E. Campbell, M. Burley, J. Dean, T. W. Clyne, *Mater. Sci. Eng. A* **2022**, *848*, 143429.

[7] Y. C. Zhang, M. C. Li, H. Y. Bi, J. Q. Gu, D. X. Chen, E. Chang, W. Zhang, *Mater. Sci. Eng. A* **2018**, *724*, 411.
[8] M. H. Zhang, H. Y. Chen, Y. K. Wang, S. J. Wang, R. G. Li, S. L. Li, Y. D. Wang, *J. Mater. Sci. Tech.* **2019**, *35*, 1779.
[9] T. W. Mukarati, R. J. Mostert, C. W. Siyasiya, *Mater. Sci Eng. A* **2020**, *792*, 139741.
[10] T. Masumura, T. Tsuchiyama, *ISIJ Int.* **2021**, *61*, 617.
[11] X. Deng, G. B. Piotrowski, J. J. Williams, N. Chawla, *Int. J. Fatigue* **2005**, *27*, 1233.
[12] N. Chawla, B. Jester, D. T. Vonk, *Mater. Sci. Eng. A* **2003**, *346*, 266.
[13] A. L. Gurson, *J. Eng. Mater. Tech. Trans ASME* **1977**, *99*, 2.
[14] M. Trillat, J. Pastor, *Eur. J. Mech. A Solids* **2005**, *24*, 800.
[15] M. Trillat, J. Pastor, P. Thore, *C. R. Mec.* **2006**, *334*, 599.
[16] J. B. Leblond, L. Morin, *J. Appl. Mech. Trans ASME* **2014**, *81*, 051012.
[17] L. Morin, J. B. Leblond, V. Tvergaard, *J. Mech. Phys. Solids* **2016**, *94*, 148.
[18] I. Holte, C. F. Niordson, K. L. Nielsen, V. Tvergaard, *Eur. J. Mech. A Solids* **2019**, *75*, 472.
[19] H. Shen, L. C. Brinson, *Int. J. Solid. Struct.* **2007**, *44*, 320.
[20] T. W. Clyne, J. E. Campbell, M. Burley, J. Dean, *Adv. Eng. Mater.* **2021**, 21004037.
[21] Y. T. Tang, J. E. Campbell, M. Burley, J. Dean, R. C. Reed, T. W. Clyne, *Materialia* **2021**, *15*, 101017.
[22] M. Ziaee, N. B. Crane, *Addit. Manufact.* **2019**, *28*, 781.
[23] N. Tuncer, A. Bose, *JOM* **2020**, *72*, 3090.
[24] J. E. Campbell, M. Gaiser-Porter, W. Gu, S. Ooi, M. Burley, J. Dean, T. W. Clyne, *Adv. Eng. Mater.* **2022**, 2101398.